Journal of Colloid and Interface Science 597 (2021) 223–232

Contents lists available at ScienceDirect

Journal of Colloid and Interface Science

journal homepage: www.elsevier.com/locate/jcis

Regular Article

Multivalent counterion induced multilayer adsorption at the air-water interface in dilute Aerosol-OT solutions

Zi Wang [a,b], Peixun Li [b], Kun Ma [b], Yao Chen [b], John R.P. Webster [b], Mario Campana [b], Zifeng Yan [a,*], Jeff Penfold [b,c,*], Robert K. Thomas [c]

[a] School of Science, State Key Laboratory of Heavy Oil Processing, China University of Petroleum, Qingdao 266580, China
[b] ISIS Facility, Rutherford Appleton Laboratory, STFC, Chilton, Didcot, Oxon OX11 0QX, UK
[c] Physical and Theoretical Chemistry Laboratory, Oxford University, South Parks Road, Oxford OX1 3QZ, UK

GRAPHICAL ABSTRACT

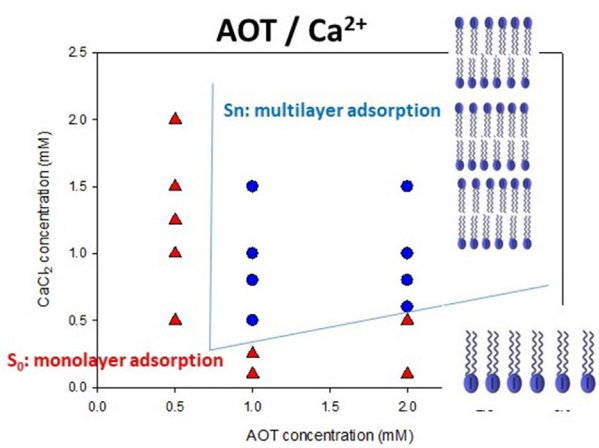

ARTICLE INFO

Article history:
Received 5 March 2021
Revised 29 March 2021
Accepted 30 March 2021
Available online 8 April 2021

Keywords:
Surface multilayer formation
Multivalent counterions
Aerosol-OT
Air–water interface
Anionic surfactants

ABSTRACT

The formation of surface multilayer structures, induced by the addition of multivalent counterions in dilute surfactant solutions, has been widely observed in a range of anionic surfactants. The phenomenon is associated with the ability to manipulate surface properties, especially in the promotion of enhanced surface wetting, and in the presence of an extensive near surface reservoir for rapid surface delivery of surfactant and other active components.

Hypothesis.

In the single alkyl chain anionic surfactants, such as sodium dodecysulfate, SDS, sodium alkylethoxylsulfate, SAES, and alkylestersulfonate, AES, surface multilayer formation is promoted by trivalent counterions such as Al^{3+}, and is generally not observed with divalent counterions, such as Ca^{2+} or with monovalent counterions. In the di-alkyl chain anionic surfactant, dodecylbenzenesulfonate, LAS, surface multilayer formation now occurs in the presence of divalent counterions. It is attributed to the closer proximity of a bulk lamellar phase, resulting in a greater tendency for surface multilayer formation, and hence should occur in other di-alkyl chain anionic surfactants.

* Corresponding authors at: ISIS Facility, Rutherford Appleton Laboratory, STFC, Chilton, Didcot, Oxon OX11 0QX, UK (J. Penfold).
E-mail addresses: zjgancat@upc.edu.cn (Z. Yan), jeff.penfold@stfc.ac.uk (J. Penfold).

https://doi.org/10.1016/j.jcis.2021.03.183
0021-9797/© 2021 Elsevier Inc. All rights reserved.

Experiments.

Aerosol-OT, AOT, is one of the most commonly used di-alkyl chain anionic surfactants, and is extensively used as an emulsifying, wetting and dispersing agent. This paper reports on predominantly neutron reflectivity, NR, measurements which explore the nature of surface multilayer formation of the sodium salt of AOT at the air-solution interface with the separate addition of Ca^{2+} and Al^{3+} counterions.

Findings.

In the AOT concentration range 0.5 to 2.0 mM surface multilayer formation occurs at the air-solution interface with the addition of Ca^{2+} or Al^{3+} counterions. Although the evolution in the surface structure with surfactant and counterion concentration is broadly similar to those reported for SDS, SAES and AES, some notable differences occur. In particular the surfactant and counterion concentration thresholds for surface multilayer formation are higher for Ca^{2+} than for Al^{3+}. The differences encountered reflect the greater affinity of the di-alkyl chain structure for lamellar formation, and how the surface packing is controlled in part by the headgroup structure and the associated counterion binding affinity.

© 2021 Elsevier Inc. All rights reserved.

1. Introduction

The formation or adsorption of surfactant multilayers at the air-water interface from dilute solution, induced by the addition of multivalent counterions, oligoions or polyions, has been extensively demonstrated, using predominantly neutron reflectivity [1,2]. Macroscopically the surface multilayer formation is associated with enhanced wetting characteristics [3]. It provides the opportunity to manipulate wetting properties in many diverse applications. The surface multilayer structures also provide an efficient near surface reservoir for rapid, enhanced and prolonged delivery of other active agents in formulations, for example, in perfume delivery [4,5]. Furthermore it offers greater opportunities for improved solubilisation properties and more effective emulsification. Importantly these new functionalities in wetting, and enhanced surface delivery extend beyond the air-solution interface and have potentially greater importance at the solid-liquid and liquid-liquid interfaces. It has the potential for implementation over a wide range of product sectors, in pesticides, enhanced oil recovery, bio-lubrication and home and personal care products.

The surface multilayer formation at the air-water interface at low surfactant concentrations has now been extensively reported for a range of different anionic surfactants, in the presence of the trivalent counterions, Al^{3+}, other trivalent counterions, and mixtures of multivalent counterions. The role of headgroup geometry, alkyl chain length and geometry, and surfactant mixing, has been investigated [6–15]; and the systems investigated include sodium dodecylsulfate, SDS, sodium alkylethoxylsulfate, SAES, and alkylestersulfonate, AES, surfactants. These studies illustrated how the alkyl chain structure affects the packing, and how the headgroup structure affects the packing and relative counterion binding strengths. The surface structure evolves from a monolayer, S_0, to a range of different multilayer structures, which depend upon the structural features of the surfactant and the relative surfactant and counterion concentrations. Beyond the formation of a single monolayer, S_0, structures with typically 1 to 3 bilayers beneath that initial monolayer and separated by thin hydrated layers, and S_1-S_3 structures have all been observed. Beyond that, with increasing surfactant and counterion concentrations extended multilayer structures, S_n, are formed; where n is the number of bilayers adsorbed beneath the initial monolayer. In some cases the number of bilayers can be identified from the data, where $n \leq 10$; but for large n instrumental resolution and disorder means that n cannot be accurately determined, and such structures are designated S_m. The strong in-plane counterion binding between neighbouring surfactant molecules, which reduces preferred curvature, and bridging across layers, promote the attractive interaction required for the surface multilayer formation. Although predominantly investigated at the air-water interface, it has also been observed and reported at the hydrophobic and hydrophilic solid-solution interfaces [3,16,17].

At higher surfactant concentrations, both anionic and cationic di-alkyl chain surfactants form lamellar phases, L_α, and complex phase diagrams evolve with surfactant concentration, temperature and electrolyte concentration. The basic lamellar phase can exist as a concentrated or space filling lamellar phase, $L_\alpha(c)$ or $L_\alpha(sf)$, swollen lamellar phase, $L_\alpha(sw)$, as vesicles and bicontinuous structures. At these higher surfactant concentrations the concentrated or swollen lamellar phases can preferentially adsorb to interfaces, and this has been observed for a range of systems at the air-solution [18–21] and solid-solution [20–24] interfaces. Penfold et al. [18] reported the adsorption of a $L_\alpha(c)$ lamellar structure at the air-water interface for the di-alkyl chain cationic surfactant dihexadecyldimethylammonium bromide in NaBr, and observed a $L_\alpha(c)$ to $L_\beta(c)$ transition at the surface with temperature. Li et al. [19–21], McGillivray et al. [22] and Hellsing et al. [24] have reported on the structure of swollen lamellar phases in Aerosol-OT and didodecyldimethylammonium bromide and variants, with relatively large bilayer spacings, at both the air-solution and solid-solution interfaces.

It is postulated the closer proximity of a bulk lamellar phase offers a greater opportunity for surface multilayer formation in the presence of multivalent counterions. This was demonstrated by Tucker et al. [25–27] for the alkylbenzenesulfonate, LAS, anionic surfactant at the air-water interface, in the presence of Ca^{2+} divalent counterions [25]. Unlike the single chain anionic surfactants discussed earlier, SDS, SAES and AES surfactants, divalent and not trivalent counterions are sufficient to induce surface layering in dilute LAS solutions. Apart from the role of surfactant and counterion concentration, the impact of a nonionic cosurfactant to disrupt the divalent counterion binding was demonstrated [25,26]. Tucker et al. [27] also investigated the role of the alkyl chain structure, with different LAS isomers, on the nature of the surface multilayer formation induced by Ca^{2+} counterions. Some differences in the counterion induced multilayer formation between the single and di-alkyl chain anionic surfactants exist. Notably trivalent counterions are required for the single alkyl chain surfactant, but divalent counterions are sufficient for the di-alkyl chain surfactants. Furthermore, in the di-alkyl chain surfactant in the presence of Ca^{2+} the intermediate layered structures, S_2-S_4, seem less prevalent, and the S_n structures have generally lower values of n. The differences observed between the formation of surface multilayer structures in the presence of Ca^{2+} for LAS compared with the Al^{3+} induced surface layering in the single alkyl chain anionic surfactants raises the interesting possibility of surface multilayer formation in the presence of lower valence counterions in other anionic di-alkyl chain surfactants.

Exploring the surface multilayer formation in the presence of multivalent counterions for a wider range of di-alkyl chain anionic surfactants is the purpose of this study. The particular focus of this paper is on the tendency of the sodium salt of Aerosol-OT, AOT, to form surface multilayers at the air-solution interface in dilute solution in the presence of either Ca^{2+} or Al^{3+} counterions.

AOT, Aerosol-OT, sodium (2-ethylhexyl) sulfosuccinate, is one of the most commonly used anionic surfactants, with widespread applications in the stabilisation of emulsions and microemulsions, as a wetting and dispersing agent, in solubilisation and the formation of inverse structures [28–30]. These properties are widely associated with the 'wedge' structure of AOT [31], which arises from the ethyl-hexyl branched di-alkyl chain structure and the sulfosuccinate headgroup, as shown in Fig. 1.

The solution structure of AOT has been extensively studied [32–38]. The regions of L_α, L_α(sw), sponge phase, L_3, and the L_α(sw)/L_1 and L_3/L_1 coexistence regions (where L_1 is a dilute isotropic micellar phase) have all been quantified as a function of concentration, temperature and salt concentration, in the concentration region of a few wt % (~2 to 20 mM).

The nature of the monolayer adsorption of AOT at the air-water interface has been studied [39,40] and particular emphasis on the role of Ca^{2+} impurities on the adsorption was made. Despite the strong binding of Ca^{2+} due to the chelating effect of the ester carboxyl group adjacent to the sulfonate group, tetrasodium ethylenediaminetetraacetate, EDTA, was shown to be an effective sequestering agent. Bilayer adsorption from dilute solution and the adsorption of a lamellar phase at more concentrated solution have, as discussed earlier, been demonstrated at different solid-solution interfaces [16,17,19–21,23,24].

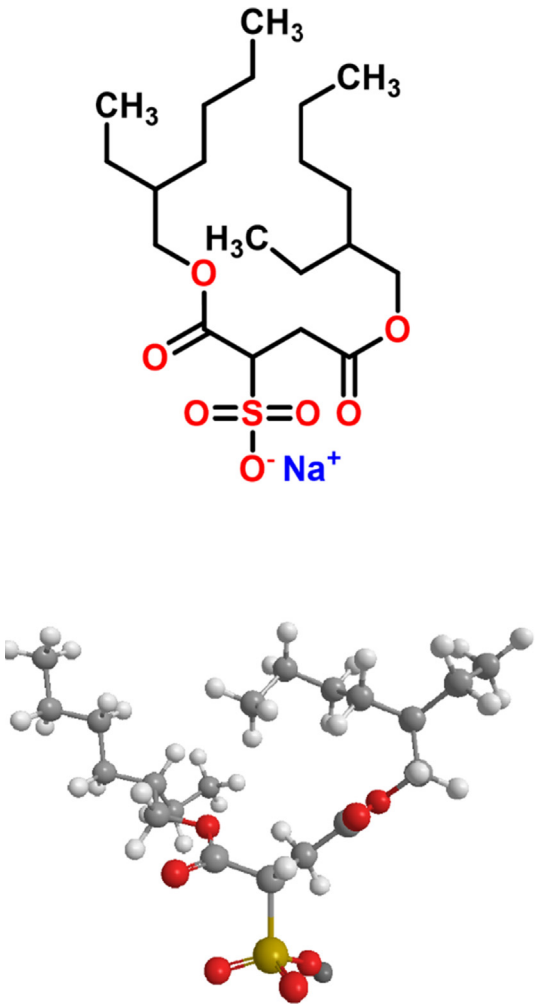

Fig. 1. Molecular structure of AOT.

Apart from the studies on LAS [25–27], most of the demonstrations of surface multilayer formation have been with single alkyl chain anionic surfactants [6–15]. Hence it is important to extend the investigations to other di-alkyl chain anionic surfactants. Given the particular and special structure of AOT, its unique properties and widespread applications, AOT offers potential new characteristics and opportunities. Hence in this paper neutron reflectivity, NR, has been predominantly used to investigate and characterise the nature of AOT adsorption at the air-solution interface, at solution concentration in the range 0.5 to 2 mM, and in the presence of either Ca^{2+} of Al^{3+} counterions.

2. Experimental details

The surface properties of AOT at the air-water interface in the presence of $CaCl_2$ and $AlCl_3$ were evaluated using neutron reflectivity, NR, and surface tension, ST. The NR measurements were made at 3 surfactant concentrations, 0.5, 1.0 and 2.0 mM; in $CaCl_2$ concentrations from 0.1 to 2 mM, and in $AlCl_3$ concentrations from 0.01 to 1 mM. Surface tension measurements were made in H_2O, 100 mM NaCl, 0.5 $AlCl_3$, and 0.5 mM $CaCl_2$.

(a) Surface tension

The surface tension measurements were made using a Kruss K11 maximum pull tensiometer. The platinum plate of the tensiometer was rinsed in high purity water and dried in a Bunsen flame between each measurement, and the tensiometer was calibrated to a surface tension of 72 mNm^{-1} for pure water. The temperature was controlled at 25 ± 1 °C. Each measurement in a dilution series, from a concentration above the critical micelle concentration, cmc, was repeated until the variation in the surface tension was $\leq$ 0.1 mN m^{-1}. The average of the measured values at each concentration is plotted, and the associated error at each point is $\leq$ 0.1 mNm^{-1}.

(b) Neutron reflectivity

The neutron reflectivity measurements were made on the CRISP and SURF reflectometers [41,42] at the ISIS pulsed neutron source. The reflectivity, R (Q), measurements at the air-water interface were made using the 'white beam time of flight' method to cover a wide range of Q values simultaneously. Q is the wave vector transfer perpendicular to the surface and is defined as $Q = 4\pi\sin\theta/\lambda$, θ is the grazing angle of incidence of 1.5° and λ is the neutron wavelength. Neutron wavelengths in the range ~ 1 to 7 Å were used to cover a Q range ~ 0.045 to 0.35 $Å^{-1}$. The high Q limit is determined by the point at which the reflected signal is comparable to the background signal, arising from the incoherent scattering from the aqueous sub-phase. The reflectivity is normalised to an absolute scale by reference to the direct beam and the reflectivity from a known surface, D_2O using standard procedures [41,42].

The samples were contained in 25 ml sealed Teflon troughs, controlled at 25 °C, and measured sequentially on a 5 position sample changer. Each measurement was repeated at least 3 times until the reflectivity no longer changes. From an individual measurement time ~ 40 mins this resulted in a total lapse time of up to 4–8 h.

(c) Materials

High purity D_2O, NaCl, $CaCl_2$, $AlCl_3$ (analytical grade) were obtained from SIGMA and used as supplied. High purity H_2O, from an Elga Ultrapure system with a resistivity of 18.2 MΩ cm, was used. All glassware, Teflon troughs and containers associated with sample preparation, NR and ST measurements were cleaned in alkali detergent, Decon90, and rinsed extensively in high purity water.

The protonated AOT ($(C_8H_{17}OOC)_2C_2H_3SO_3Na$), abbreviated h-AOT, was obtained from SIGMA, and purified as described elsewhere [44]. The deuterium labelled AOT ($(C_4H_{17}OOC)(C_2D_5)CD_2OOC)_2C_2H_3SO_3Na$), abbreviated d-AOT, was synthesised and purified by the ISIS Deuterium Facility [43], using the procedures described in detail elsewhere [44]. The purity of both surfactants was assessed by ST, illustrated by an absence of a minimum at the cmc, and by NMR, to a purity > 99%.

The ST measurements were made using h-AOT in H_2O. The NR measurements were made using d-AOT in null reflecting water, nrw, 8 mol% D_2O/92 mol% H_2O mixture, with a scattering length density or refractive index equal to air, 1.0.

3. Results and discussion

(a) Surface tension

The surface tension was measured for h-AOT in H_2O, in 100 mM NaCl, $CaCl_2$ and $AlCl_3$. The surface tension data for AOT and AOT in 100 mM NaCl are shown in Fig. 2a, and the impact of $CaCl_2$ and $AlCl_3$ on the surface tension are shown for comparison in Fig. 2b.

The surface tension behaviour of AOT, in NaCl, and $CaCl_2$ are broadly similar to that previously reported for AOT [39,40]. The cmc for AOT was determined from Fig. 2 as ~ 3.7 mM, and in the presence of NaCl, $CaCl_2$ and $AlCl_3$ the cmc decreased to ~ 0.2, 0.8 and 0.2 mM respectively. The impact of impurities, and particularly Ca^{2+}, on the surface tension of AOT has been discussed and evaluated at length elsewhere [39,40,45]. The strong binding of Ca^{2+} impurities impacts directly upon the form of the surface tension and the ability to estimate reliable adsorbed amounts [40,45], and neutron reflectivity has been shown to provide a more consistent and accurate evaluation. However the addition of the different electrolytes here have a profound impact upon the cmc values.

The impact of Al^{3+} on the surface tension of anionic surfactants, and notably the SAES and AES surfactants [7,8,11–15], has been previously demonstrated. The main features were a significant reduction in the cmc and a reduction in the minimum or limiting surface tension value. In general for these surfactants, as the surface tension measurements are made at a fixed Al^{3+} concentration and variable surfactant concentration, the surface tension increases again towards the limiting value in the absence of electrolyte when the surfactant concentration in well in excess of the Al^{3+} concentration, as illustrated elsewhere [7,8,11]. From the surface tension data for the SAES surfactants in the presence of Al^{3+}, Thomas et al. [46] were able to correlate the surface tension variations in the region between the cmc's in the presence and absence of Al^{3+} to the associated solution phase behaviour and the role of phase separation in such solutions. Although the ST data per se shows no direct indication, Thomas et al. [46] have demonstrated that this region also correlates with the onset of surface multilayer formation.

For AOT, although the expected decrease in the cmc in the presence of NaCl, $CaCl_2$ and $AlCl_3$ is observed in Fig. 2, the minimum or limiting values of the surface tension do not change significantly. This is quantitatively different to what was reported for the SAES, AES surfactants [7,8,11] and for SDS [45]. This is because the limiting surface tension for AOT is already relatively low in the absence of electrolyte. This may be due in part to the strong binding of impurity ions such as Ca^{2+}, as discussed earlier. However it has been shown that the limiting surface tension was not significantly affected even in the presence of the chelating agent ethylenediaminetetraacetic acid, EDTA [39,40]. Hence the low surface tension for AOT is associated with the more efficient packing of the alkyl chains of AOT at the interface, with area/alkyl chain $\leq$ 35 Å^2. Furthermore the packing factor associated with AOT disfavours micellisation, and this further promotes the reduction in the surface tension with increasing surfactant concentrations, as shown in Fig. 2. However, as previously show in other anionic surfactants in the presence of multivalent counterions [46], the ST data does provide an important indicator of the region where surface multilayer formation is likely to occur.

(b) Neutron reflectivity

Neutron reflectivity measurements were made at the air-water interface at three different AOT concentrations, for d-AOT in nrw, and at a range of $CaCl_2$ and $AlCl_3$ concentrations, from 0.1 to 2 mM for $CaCl_2$, and from 0.01 to 1.0 mM for $AlCl_3$. The data shown in Fig. 3a for 2 mM AOT/$CaCl_2$ and in Fig. 3b for 2 mM AOT/$AlCl_3$ illustrate the main structural features observed.

In the presence of $CaCl_2$ two main surface structures are observed. At the lowest surfactant concentration, 0.5 mM, and at low $CaCl_2$ concentrations at higher surfactant concentrations, 1 and 2 mM, the adsorbed surface layer is a single monolayer, S_0, characterised by a simple monotonic curve. At the higher surfactant concentrations, 1 and 2 mM, and for $CaCl_2$ concentrations $\geq$ 0.5 mM the surface structure is different. The reflectivity exhibits a broad Bragg peak at a Q value ~ 0.2 Å^{-1} and contains interference fringes at lower Q values arising from the total thickness of the surface layer. As previously demonstrated [1,2,7–15,25–27] this is consistent with the adsorption of a multilayer structure, S_n, at the surface.

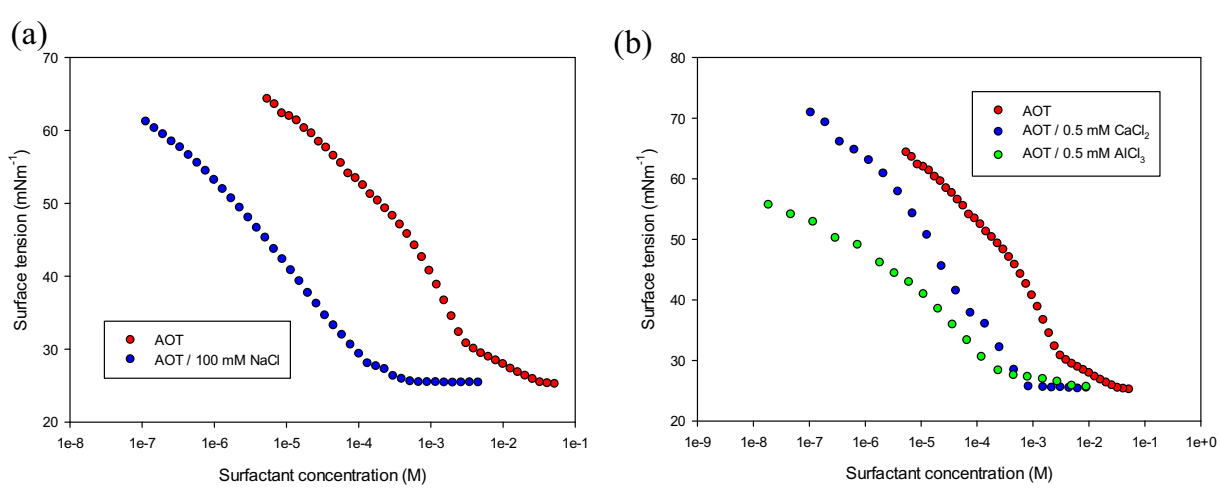

Fig. 2. Surface tension for (a) h-AOT in H_2O and in 100 mM NaCl, (b) h-AOT in H_2O, 0.5 mM $CaCl_2$, and 0.5 mM $AlCl_3$.

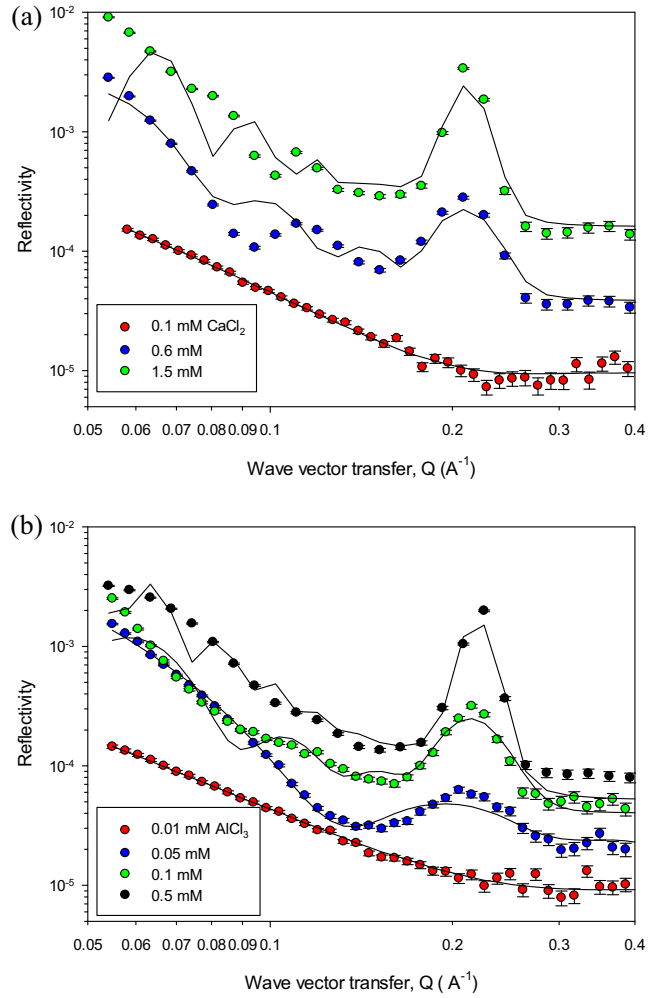

Fig. 3. Neutron reflectivity versus wave vector transfer, Q, for (a) 2 mM AOT/$CaCl_2$, and (b) 2 mM AOT/$AlCl_3$. In Fig. 3 a and b each curve is shifted vertically with respect to the previous curve by a factor x4 and x2 respectively. The solid lines are model fits to the data, as described in the main text and for the key model parameters summarised in Tables S1 and S2 in the Supporting Information.

In the presence of $AlCl_3$ the structural variations at the surface are slightly different and richer, as illustrated in Fig. 3b. In this case three different surface structural forms are observed. At low $AlCl_3$ concentrations, and at all three surfactant concentrations explored, the reflectivity is consistent with monolayer adsorption. At intermediate $AlCl_3$ concentrations, in the range 0.05 to 0.1 mM, the reflectivity has a single broad interference fringe at a Q ~ 0.2 Å^{-1}, consistent with an S_1 structure, comprising a monolayer at the air-water interface and a single bilayer beneath the initial monolayer. At higher $AlCl_3$ concentrations a broad Bragg peak at a Q ~ 0.2 Å^{-1} is again indicative of a multilayer structure at the interface.

A quantitative analysis of the structural details of the three main regions, S_0, S_1, and S_n follows. The difficulties in obtaining an accurate representation of the structure of the S_n region due to different forms of the structural disorder are highlighted in Fig. 3. In particular the region in the reflectivity at Q values below the Bragg peak is only approximately modelled, as a result of using a simplified model. The impact and nature of the structural disorder is discussed in detail later in the paper, and use of a simplified model justified.

In the meantime, from these structural variations an approximate surface phase diagram has been constructed, as shown for $CaCl_2$ and $AlCl_3$ in Fig. 4 a and b.

With the addition of $CaCl_2$ and $AlCl_3$, at all three AOT concentrations, there are regions of monolayer adsorption, which are more extensive with the addition of $CaCl_2$ than for $AlCl_3$. The reflectivity data for the monolayer adsorption are analysed using the exact equation for a deuterated monolayer on a nrw subphase, of the form [47],

$$R(Q) = \frac{16\pi^2}{Q^4}(2\rho)^2 \sin\left(\frac{Qd}{2}\right)^2 \quad (1)$$

where d and ρ are the thickness and scattering length density of the adsorbed layer. The adsorbed amount is then directly related to the product d.ρ, assuming a layer of uniform composition [47],

$$A = \sum b/d\rho \quad \Gamma = 1/NaA \quad (2)$$

where $\sum b$ is the scattering length of the adsorbed species (3.97×10^{-3} Å for d-AOT), A is the area/molecule, Γ is the adsorbed amount in mol cm^{-2}, and Na is Avogadro's number.

In the monolayer region the key model parameters which are refined are d and ρ, and those parameters and derived adsorbed amounts for the AOT monolayer adsorption in $CaCl_2$ and $AlCl_3$ are summarised in Tables S1a and S2a in the Supporting Information. The mean thickness, <d>, averaging over the $CaCl_2$ and $AlCl_3$ data, is 19 ± 2 Å; broadly consistent with previous observations [39,40]. The mean area/molecule at the cmc was previously deter-

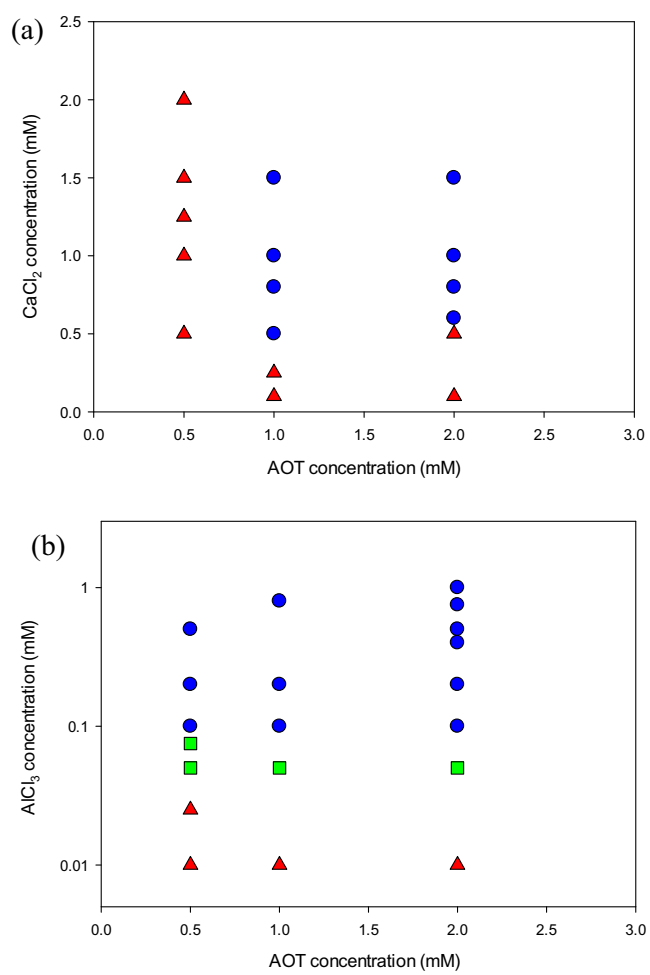

Fig. 4. Surface phase diagram as a function of surfactant and electrolyte concentration for (a) AOT/$CaCl_2$, (b) AOT/$AlCl_3$. The red triangles are S_0, green squares, S_1, and the blue circles are S_n, and are the points at which reflectivity measurements were made. (For interpretation of the references to colour in this figure legend, the reader is referred to the web version of this article.)

mined for AOT as 78 Å^2 and for Ca-AOT as 68 Å^2 [39,40]. The mean area/molecule determined here for AOT in the presence of $CaCl_2$ was 67 ± 3 Å^2, and in the presence of $AlCl_3$ was 72 ± 3 Å^2. This represents an increase in the adsorption with the addition of $CaCl_2$ ~ 15% and ~ 8% for the addition of $AlCl_3$. These increases are comparable to those previously reported for the SAES and AES surfactants with the addition of electrolyte [11,14,15,48]. A significantly larger change was reported for SDS [48], and the relative change is associated with the level of dissociation of the surfactant. The SAES and AES surfactants were observed in general to exhibit a lower degree of dissociation and a stronger counterion binding. However the results reported here for AOT are associated with the intrinsic closer packing in the monolayer for AOT, where the area/alkyl chain is ≤ 35 Å^2, which mitigates against a significant increase in the packing (reduction in the area/molecule) in the presence of electrolyte.

Furthermore the differences between the impact of $CaCl_2$ and $AlCl_3$ are in part due to the differences in ionic strength of the added $CaCl_2$ and $AlCl_3$, which is typically greater than a factor 10 for Ca^{2+} compared to Al^{3+} in the regions where monolayer adsorption exists.

The reflectivity data in the presence of $AlCl_3$ has a narrow region at $AlCl_3$ concentrations ~ 0.05 mM where the reflectivity is characterised by a single broad interference fringe. The simplest model consistent with the data, as illustrated elsewhere for the SAES and AES surfactants [6–15], comprises of three layers. This is described as the S_1 structure, and is interpreted as an initial monolayer at the air-water interface with a bilayer adsorbed beneath the monolayer and separated by a thin layer comprising primarily of solvent and surfactant headgroups. The data are hence modelled using the optical matrix formulism [49], in which the minimum number of layers and refinable parameters; that is, the simplest model consistent with the data, is used. The key model parameters that are refined are the thicknesses and scattering length densities of each layer, d_i, ρ_i, and these are summarised in Table S2b in the Supporting Information. Although a relatively simple NR profile, comprising of a single broad interference fringe, due to the inherent disorder it is relatively difficult to model, and this is reflected in a relatively large spread in the values in Table S2b. However the mean thicknesses of the three layers are 18 ± 2, 12 ± 4, and 18 ± 2 Å respectively; and are broadly consistent with those reported for related structures [6–15], and with the model of a monolayer and bilayer separated by a thin solvent layer.

The appearance of a Bragg peak at a Q ~ 0.2 Å^{-1} is consistent with the adsorption of multilayers at the interface, S_n, in the presence of $CaCl_2$ and $AlCl_3$ at higher surfactant and electrolyte concentrations. The broad Bragg peak and the occurrence of interference fringes in the lower Q region are consistent with a finite number of bilayers adsorbed, n ≤ 10. However at higher surfactant and electrolyte concentrations the Bragg peak narrows and the interference fringes are no longer visible. This occurs when the number of bilayers adsorbed is greater, for n ≥ 20. The simplest model which encapsulates the main features is used to analyse the data, in which the surface is represented by a series of identical bilayers. In the kinematic approximation this can be expressed by a simple recursive relationship, as developed by Tidswell et al. [50] and Sinha et al. [51], such that,

$$R(Q) = \frac{16\pi^2}{Q^2}\left|\sum_{i=0}^{N}(\rho_i - \rho_{i+1})\exp(-iQd_i)\exp\left(-Q^2\sigma_i^2/2\right)^2\right| \quad (3)$$

where ρ_i is the scattering length density of the ith layer, i = 0 represents the subphase, d_i is the distance to the interface between the ith and i-1th layers from the subphase, $d_i = \sum_{j=0}^{k} l_j$, l_j is the thickness of the jth layer, $\rho_{(N+1)}$ is the scattering length density of the upper phase (air), N is the number of layers, N/2 (or n) is the number of bilayers, and σ_i is the roughness between the ith and i + 1th layers.

This simple bilayer model has been extensively applied to a range of surfactant bilayer structures at the air-water interface [6–15,25–27]. Although the formulism provides flexibility in the variation in the bilayer parameters, generally it has been applied on the assumption that the structure is invariant from bilayer to bilayer, and that the interfacial roughness is minimal; and the same assumptions are made in its initial application here. However the width of the Bragg peak is generally broader than the expected 1/n dependence and the total thickness interference fringes are damped to a greater or lesser degree. This implies a degree of disorder, both laterally and vertically, in the surface structure. The broadening of the Bragg peak and the damping of the interference fringes are in part due to the instrumental resolution, ΔQ, which is incorporated into the model. However the instrumental resolution is typically ~ 0.05, and the ΔQ values obtained are typically larger (see Tables S1b, S2c and S3 in the Supporting Information). ΔQ is treated as a variable and the additional contribution, over and above the instrumental resolution, is used to model some aspects of the surface disorder. It is assumed that the surface consists of domains of multilayer structures and that the additional contribution to ΔQ is associated with the mosaic of the orientational distribution of those patches.

In broad terms the simple multilayer model encapsulates the main features of the AOT data, as shown in Fig. 3a and b; consistent with the observations on a range of related systems [6–15,25–27]. The key model parameters for the multilayer structures for AOT in $CaCl_2$ and $AlCl_3$ are summarised in Tables S1b and S2c in the Supporting Information. For the multilayer structures consistent with a larger number of bilayers, n ≥ 10–20 the data are most sensitive to 2d, ($d_1 + d_2$), and Δρ, (ρ_1-ρ_2). Furthermore the ΔQ term ensures that the interference fringes are effectively damped and the width of the Bragg peak accounted for. However it is difficult in this regime to be precise about the value of n, other that it is relatively large. For the multilayer structures where n ≤ 10 the occurrence of the total thickness fringes can enable the number of bilayers to be determined with greater certainty. In the modelling presented here the key adjustable parameters are hence d_1, ρ_1, d_2, ρ_2, N and ΔQ. However, as discussed earlier, it is often 2d, Δρ, N and ΔQ which are most readily accessible and to which the data are most sensitive to. In the data presented here and in the tables of parameters in the Supporting Information 2d is relatively constant and the main variations occur in Δρ, N, and ΔQ, as the visibility of the Bragg peak and definition of the multilayer structure varies. Without introducing further complexities, the model adequately describes the main features of the structures observed, see Fig. 3.

However the model fits are not perfect due to the disorder in the structure. This is especially revealed in the ability to model the total thickness interference fringes that occur at Q values below the Bragg peak. Hence further potential sources of the disorder associated with the structures and how they affect the reflectivity profile, and especially the total thickness fringes, are explored in the more detail in the following discussion.

A major source of potential disorder in the surface multilayer structures is the time dependence of the evolution of the surface structure. That is, different regions of the surface may evolve on different time scales. Although the experimental procedures adopted are designed to ensure equilibrium structures are achieved, the timescales are relatively long and some uncertainty can still exist. Fig. 5 shows an example of how the surface structure can evolve with time, for 2 mM AOT in 1.5 mM $CaCl_2$, for an initial measurement immediately following sample transfer and after 240 and 480 min respectively.

From the visual trends in the reflectivity profiles and from the model parameters, the multilayer structure at the interface is

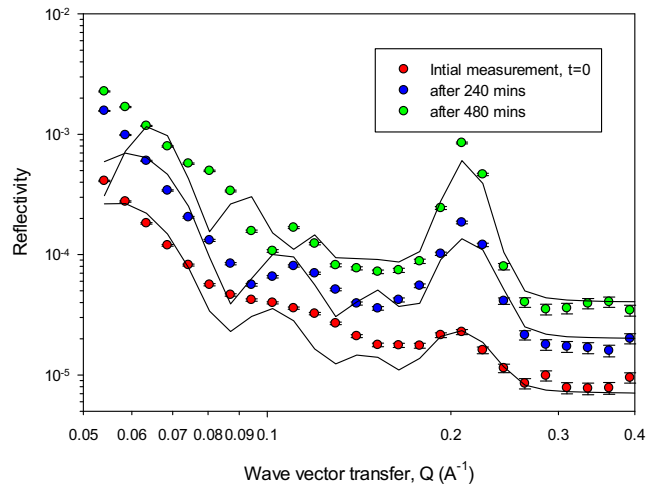

Fig. 5. Neutron reflectivity versus wave vector transfer, Q (Å^{-1}), for 2 mM AOT in 1.5 mM $CaCl_2$, measured at different times, over a period ~ 500 mins. See legend for details. Each curve is shifted vertically with respect to the previous curve. The solid lines are model calculations, as described earlier, and for the key model parameters summarised in Table S3 in the Supporting Information.

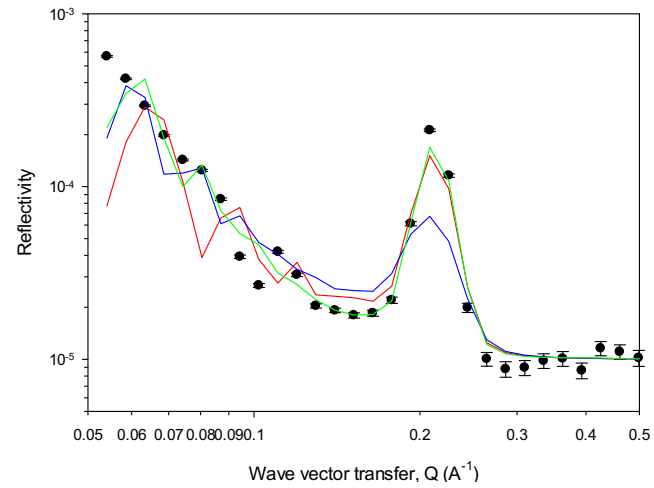

Fig. 6. Neutron reflectivity data for 2 mm AOT/1.5 mM $CaCl_2$, at T = 480 mins (see also Figs. 3 and 5). (a) Solid red line is multilayer model fit (as described in the main text) for d_1 = 15 Å, d_2 = 14.5 Å, ρ_1 = 5.5x10^{-6}Å^{-2}, ρ_2 = 1.0x10^{-6}Å^{-2}, n = 12, ΔQ = 0.12. (b) Solid blue line, as (a) with η = 250 Å, and (c) solid green line, as (a) with modified 1st bilayer, d_1 = 14 Å, d_2 = 14 Å, ρ_1 = 4e^{-6}, ρ_2 = 2e^{-6}. (For interpretation of the references to colour in this figure legend, the reader is referred to the web version of this article.)

broadly similar with time, but there is an increase in the intensity of the Bragg peak with time. From the modelling this is initially interpreted as an increase in the contrast between the two layers in the bilayer structure, as the structure becomes ordered (see Table S3 in the Supporting Information). This eventually results in a modest increase in the number of bilayers adsorbed at the interface being required to account for the increasing intensity of the Bragg peak.

The use of ΔQ to incorporate the effect of instrumental resolution on the reflectivity from the multilayer structures and to simulate the effects of orientational distributions of lamellar fragments at the interface was discussed earlier. From the parameters in Table S3 and in Tables S1b and S2c in the Supporting Information for similar data, show that the contribution from ΔQ is large when the number of bilayers, n, is relatively low; and generally decreases when n is large, $\geq$20. This implies a greater degree of ordering and greater surface coverage associated with a growth of the fragments towards fuller coverage.

It has been demonstrated elsewhere that model fitting using approaches such as maximum entropy minimisation [52] can be used to provide a comprehensive modelling of the complex reflectivity profiles that arise in such systems [21,22,3]. This usually results in a scattering length density distribution, which then can be subject to the ambiguities and uncertainties in interpretation. Here a different approach has been adopted, in order to capture the main features and to attempt to understand the factors which contribute to the observed structure, and the impact of different potential contributions to the structural disorder.

As illustrated in Figs. 3 and 5, the incorporation of the resolution term, which in part accounts for the smearing due to instrumental resolution, and in part accommodates disorder in terms of an orientational distribution of surface lamellae, accounts for the broadening of the Bragg peak and some of the damping of the total thickness interference fringes. In Figs. 6 and 7 two further potential contributions to the surface disorder are explored in the modelling of the reflectivity data for 2 mM AOT/1.5 mM $CaCl_2$.

The same fundamental model and model parameters, as used in Figs. 3a and 5, are used for the data in Figs. 6 and 7.

In Fig. 6 the impact of two different aspects of disorder are illustrated. The impact of modifying the definition of the bilayer structure with increasing depth is illustrated, where the structure is modified by an exponential decay in the scattering length density

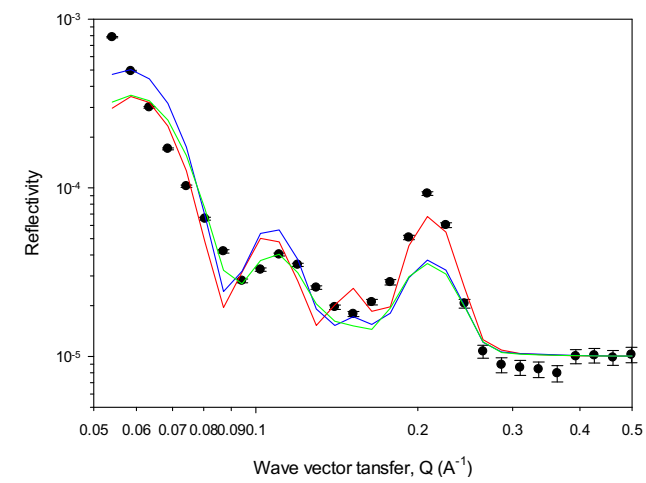

Fig. 7. Neutron reflectivity data for 2 mm AOT/1.5 mM $CaCl_2$, at T = 240 mins. (a) Solid red line is multilayer model fit (as described in the main text) for d_1 = 14.5 Å, d_2 = 14.5 Å, ρ_1 = 3.0x10^{-6}Å^{-2}, ρ_2 = 1.3x10^{-7}Å^{-2}, n = 5, ΔQ = 0.12. (b) Solid blue line, as (a) with first bilayer modified, d_1 = 14 Å, d_2 = 13 Å, ρ_1 = 2e^{-6}, ρ_2 = 1e^{-6}, (c) Green solid line, as (a) with first bilayer modified, d_1 = 13 Å, d_2 = 13 Å, ρ_1 = 2e^{-6}, ρ_2 = 1e^{-6}. (For interpretation of the references to colour in this figure legend, the reader is referred to the web version of this article.)

contrast between the two layers in the bilayer structure, of the form [25],

$$\rho_i = \rho_n - \Delta\rho\exp(-d_i/\eta) \tag{4}$$

and η is the damping coefficient.

Introducing such a damping factor effectively reduces the visibility of the total thickness interference fringes, but also markedly reduces the visibility of the Bragg peak. Incorporating an interfacial roughness, σ_i, (see Eq. (3)), produces a similar effect, and so has not been used in the analysis presented here. Shown also in Fig. 6 is the impact of changing parameters associated with just the first bilayer, adjacent to the upper air phase, in order to illustrate the effect of varying bilayer characteristics in a more controlled and limited way. Whilst having minimal impact on the Bragg peak it

is clear that such changes can effectively change the modulation of the total thickness interference fringes. In Fig. 7 the impact of modifying the first bilayer is explored further, where changes in thickness and scattering length density contrast are both explored. Although the thickness changes modulate the total thickness interference fringe pattern, changing the scattering length density contrast has a more profound impact upon the whole profile.

However, it is likely that the variations explored here occur randomly throughout the multilayer structure, and so a precise model to incorporate such effects is difficult to specify. The impact of some of the different origins of disorder has been illustrated, and highlights some of the difficulties in incorporating such defects in a meaningful way. However given the intrinsic uncertainties associated with the nature of the surface disorder, the simple model used here adequately describes the main features of the observed reflectivity profiles.

4. Discussion.

Although ST provides no direct evidence for the formation of surface multilayer structures, as discussed by Thomas et al. [46] the form of the ST data between the cmc values in the presence and absence of multivalent counterions correlate with the onset of phase separation, the solution phase behaviour and the occurrence of surface multilayer formation. The more efficient alkyl chain packing for AOT is responsible for the reduced ST variation in that region in the presence of Ca^{2+} and Al^{3+} counterions compared to the values in the absence of electrolyte, as discussed earlier. However the same correlation with the onset of surface multilayer formation exists, and so the ST data provides an important guide to the region of interest. The form of the ST data in that region also indicates that the greater surfactant packing at the interface for AOT may have an important role in the nature of the structural trends observed here.

The notable feature of the surface multilayer formation observed here for AOT is that it can be induced by the addition of either divalent (Ca^{2+}) and trivalent (Al^{3+}) counterions. For the wider range of anionic surfactants, which are mostly monoalkyl chain surfactants, in which surface multilayer formation occurs, it is not observed for the addition divalent counterions and requires the addition of trivalent counterions [1,2,6–16]. Xu et al. [11] commented that the more weakly ionic nature of surfactants such as SLES and MES are indicative of a stronger binding of Na^{+}. This implied that the stronger binding of Al^{3+}, rather than Ca^{2+}, was required to promote the surface multilayer formation. In addition to the role of trivalent counterions in binding to adjacent surfactant ions the bridging across layers to promote the surface lamellar ordering is an important factor. The exception to the need for trivalent counterions was the observation of surface multilayer formation with the addition of Ca^{2+} for the dialkyl chain LAS surfactant [25–27]. The importance of the alkyl chain geometry in surface multilayer formation has been highlighted elsewhere. Tucker et al. [27] showed that the LAS-4 isomer and the LAS-4/LAS-6 isomeric mixtures more readily form surface multilayers in the presence of Ca^{2+} than LAS-6. This was attributed to a more favourable packing of the alkyl chains for the LAS-4 isomer. In contrast, Wang et al. [14] showed that the AES surfactant with a C_{18} isostearic alkyl chain, isoC_{18}MES, did not form surface multilayer structures in the presence of Al^{3+}, unlike its straight chain equivalents such as MES, due to unfavourable alkyl chain packing [11]. For both AOT and LAS it is assumed that the denser packing of the di-alkyl chains, the preferred planar curvature, and the closer proximity of a bulk lamellar phase, enable the binding of Ca^{2+} to promote the surface layering observed.

As discussed in the Introduction, and dependent upon the structural features of the anionic surfactant, a range of surface structures from S_0 to S_n are observed. For AOT a more limited range of structures, both for the addition of Ca^{2+} and Al^{3+}, are observed (see Fig. 4). In the presence of Ca^{2+} only monolayer adsorption, S_0, and multilayer adsorption, S_n, are observed. In the presence of Al^{3+} there is an additionally a narrow region with a S_1 structure, between the S_0 and S_n regions. The other significant difference in the observed structures, compared to previous data, is that in the multilayer region, S_n, (see Fig. 4), and over much of the surfactant and counterion concentration range explored, the number of bilayers, n, is relatively small, $n \leq 10$. This contrasts with the observations for the SAES and AES surfactants, where n was generally ≥ 20. This may be because the adhesion forces are greater for the SAES and AES surfactants compared to AOT and LAS, or because of the greater intrinsic disorder for AOT and LAS. The discreet and finite nature of these multilayer structures was highlighted in a dilution experiment at the air-solution interface with 2 mM LAS/2 mM $CaCl_2$ [2], see Fig. 54 in reference 2. The dissolution of the initial multi-bilayer structure with n = 7 in a series of discreet steps (layer by layer) was observed as the bulk subphase was replaced by nrw.

A more limited range of surface structures was also observed with the AES surfactant, ethyl ester sulfonate [14]. In that case only the S_0 and S_1 structures were observed with the addition of $AlCl_3$, although S_0, S_1 and S_2 structures were observed with the addition of a mixture of $AlCl_3$ and $CaCl_2$. Similar observations were also reported for the mixtures of methyl ester sulfonate, ethyl ester sulfonate, and propyl ester sulfonates in the presence of $AlCl_3$ [15]. However, in both cases no S_n structures were observed over the range of surfactant and electrolyte concentrations investigated. These observations were attributed to impact of changing the headgroup structure on the relative counterion binding strengths of Na^{+}, Ca^{2+}, and Al^{3+}. A limited range of surface multilayer structures has been reported in some other related systems. In the C_{16} and C_{18}-MES surfactants, in the presence of Al^{3+}, only S_0 and S_1 structures were reported by Xu et al. [12]. This was attributed to the closer proximity of precipitation in these systems. A similar observation was also reported by Xu et al. [7] for the longer alkyl chain SAES surfactants, which were also closer to precipitation in the presence of multivalent counterions.

The other main feature in the AOT data is that for the addition of Ca^{2+} and Al^{3+} the threshold for the transition to the formation of S_n surface structures occurs at noticeably larger counterion concentrations for Ca^{2+}, ~ 0.5 mM, than for Al^{3+}, ~0.1 mM. This suggests that compared to Ca^{2+} the Al^{3+} binding is stronger relative to Na^{+}, and that Al^{3+} is more effective in inducing the attractive interaction required for the surface layering due to the additional bridging role between adjacent layers. The impact on the relative counterion binding strengths on the surface layering has been previously discussed [9,13–15]. Xu et al. [9] reported the ion specific effects of trivalent counterions on the surface layering and solution self-assembly in the anionic surfactant SLES. The structural variations observed correlated with the strength of the binding and the hydrated radius of the counterion, in the order Sc^{3+}, Gd^{3+}, and La^{3+}, compared to Al^{3+}. Cr^{3+} showed distinctly different effects due to a less labile hydration shell. For the AES surfactants, Xu et al. [13] investigated the role of competitive counterion adsorption on the MES surface multilayer formation. The nature of the layering depended critically upon relative binding strengths of Na^{+}, Ca^{2+}, Mg^{2+} and Al^{3+}. This relates also to the observations of Wang et al. [14,15], as discussed above, who showed how changing the AES headgroup structure impacts upon the relative counterion binding strengths. All these observations also correlate with a wider range of studies related to the effects of relative counterion binding on different phenomena in anionic surfactants, related to precipitation, flocculation, micelle growth and the evolution of the surfactant mesophases [53–57].

In some cases, where there is a richer variation in the surface structure [7,8,11], changes in those structural variations with sur-

factant and counterion concentration can be quite subtle. It is likely that the surface free energy differences associated with the different structures is quite small [57]. Hence whether certain intermediate surface phases are observed or not may be due to the sampling of the concentration space explored. The consistency of the results presented here for AOT would mitigate against such an explanation.

The limited range of structures observed, and the limited extent, in terms of the number of bilayers, of the multilayer structures may be intrinsically linked to the greater inherent disorder observed for AOT. Although the timescales for the evolution of the surface structures seem to be comparable to the previous systems studied [6–15,25–27], there may be a kinetic contribution to the disorder which is on a relatively longer timescale. There may also be an additional or alternative contribution to the disorder. The bulk phase behaviour for AOT is characterised by extensive regions of coexisting mesophases [35], where regions of L_1/L_α, L_1/L_3, and $L_1/L_\alpha/L_3$ have been identified. This suggests that the spontaneous curvature for AOT has some ambiguity. This may well manifest itself into a range of similar but different equivalent structures at the surface. However the causes of the increased disorder in the surface structures remains uncertain.

5. Conclusions

The neutron reflectivity results show the extent to which surface multilayer formation occurs at the air–water interface for dilute solutions of AOT in the presence of Ca^{2+} and Al^{3+}. The results parallel those previously reported for another dialkyl chain anionic surfactant, LAS, [25–27], in that the surface layering is induced with Ca^{2+}, as opposed to the need for trivalent counterions for a range of monoalkyl chain anionic surfactants [1,2,6–15]. The results and similarity with LAS imply that the closer proximity of a bulk lamellar phase in such systems is an important factor. Similar to the observations for LAS [25–27], the multilayer structures, S_n, have mostly a relatively low number of bilayers, and is attributed to a greater degree of disorder in the surface structures. Some potential origins of this greater structural disorder have been discussed. The differences in the Ca^{2+} and Al^{3+} concentrations required to induce the transition to the multilayer structures is associated with the relative counterion binding strengths of the different counterions and the additional role of the trivalent counterion to promote the required attractive interaction [1,2]. The limited range of surface structures observed for AOT, in the presence of Ca^{2+} and Al^{3+}, is also indicative of the role of the relative counterion binding strengths, as illustrated previously in the context of the ethyl ester sulfonates [14] and mixtures of the methyl, ethyl, and propyl ester sulfonates [15].

Finally the results further illustrate the rich opportunities for the manipulation of the surface properties in such systems, in the applications related to adjusting wetting behaviour and efficient enhanced interfacial delivery [3–5], and in enhancing emulsification and solubilisation properties [28]. The potential applications at the air-solution, solid-solution and liquid- liquid interfaces are far reaching, and cover home and personal care products, soft lubrication and bio-lubrication, pesticides, pharmaceuticals, enhanced oil recovery, and foods. The results presented here for AOT significantly extend those opportunities, and illustrate further how the surface properties can be manipulated or tailored for a specific purpose.

Declaration of Competing Interest

The authors declare that they have no known competing financial interests or personal relationships that could have appeared to influence the work reported in this paper.

Acknowledgements

The authors acknowledge the provision of the neutron beam time on the CRISP and SURF reflectometers at ISIS, and the invaluable technical and scientific support provided. The authors wish to thank the China Scholarship Council (CSC) for their financial support.

Appendix A. Supplementary material

Supplementary data to this article can be found online at https://doi.org/10.1016/j.jcis.2021.03.183.

References

[1] R.K. Thomas, J. Penfold, Multilayering of surfactant systems at the air-dilute aqueous solution interface, Langmuir 31 (2015) 7440–7456.
[2] P.X. Li, J. Penfold, R.K. Thomas, H. Xu, Multilayers formed by polyelectrolyte-surfactant and related mixtures at the air-water interface, Adv. Coll. Int. Sci. 269 (2019) 43–86.
[3] J. Penfold, R.K. Thomas, Z. Xi, H. Xu, I.M. Tucker, J.T. Petkov, D.S. Sivia, Multivalent counterion induced multilayer formation at hydrophobic and hydrophilic solid-solution interfaces, Langmuir 31 (2015) 6773–6781.
[4] R. Bradbury, J. Penfold, R.K. Thomas, I.M. Tucker, J.T. Petkov, C. Jones, Enhanced perfume delivery to interfaces using surfactant surface multilayers, J. Coll. Int. Sci. 461 (2016) 352–358.
[5] J. Penfold, R.K. Thomas, R. Bradbury, I.M. Tucker, J.T. Petkov, C. Jones, J.R.P. Webster, Perfume evaporation from the surface of aqueous surfactant-perfume mixed solutions, Coll. Surf. A 520 (2017) 178–183.
[6] J.T. Petkov, I.M. Tucker, J. Penfold, R.K. Thomas, D.N. Petsev, C.C. Dong, S. Golding, I. Grillo, The impact of multivalent counterion Al^{3+} on the surface adsorption and self-assembly of the anionic surfactant alkyl oxyethylene sulfate and anionic/nonionic surfactant mixtures, Langmuir 26 (2010) 16669–16709.
[7] H. Xu, J. Penfold, R.K. Thomas, J.T. Petkov, I. Tucker, J.R.P. Webster, The formation of surface multilayers at the air-water interface from sodium diethylene glycol monoalkyl ether sulfate/$AlCl_3$ solutions: the role of alkyl chain length, Langmuir 29 (2013) 12744–12753.
[8] H. Xu, J. Penfold, R.K. Thomas, J.T. Petkov, I.M. Tucker, J.R.P. Webster, The formation of surface multilayers at the air-water interface from sodium polyethylene glycol monoalkyl ether sulfate/$AlCl_3$ solutions: the role of the size of the polyethylene oxide group, Langmuir 29 (2013) 11656–11666.
[9] H. Xu, J. Penfold, R.K. Thomas, J.T. Petkov, I.M. Tucker, J.R.P. Webster, I. Grillo, A. Terry, Ion specific effects in trivalent counterion induced surface adsorption and solution self-assembly of the anionic surfactant sodium polyethylene glycol monododecyl ether sulfate, Langmuir 30 (2014) 4694–4702.
[10] P.X. Li, Z. Wang, K. Ma, Y. Chen, Z. Yan, J. Penfold, R.K. Thomas, M. Campana, J.R.P. Webster, A. Washington, Multivalent electrolyte induced surface ordering and solution self-assembly in anionic surfactant mixtures: sodium dodecyl sulfate and sodium diethylene glycol monododecyl sulfate, J. Coll. Int. Sci. 565 (2020) 567–581.
[11] H. Xu, R.K. Thomas, J. Penfold, P.X. Li, R.J.L. Welbourn, D.W. Roberts, J.T. Petkov, The impact of electrolyte on the adsorption of the anionic surfactant methyl ester sulfonate at the air-solution interface: surface multilayer formation, J. Coll. Int. Sci. 512 (2018) 231–238.
[12] H. Xu, P.X. Li, K. Ma, R.J.L. Welbourn, J. Doutch, J. Penfold, R.K. Thomas, D.W. Roberts, J.T. Petkov, R.L. Choo, S.Y. Khoo, Adsorption and self-assembly in methyl ester sulfonate surfactants, their eutectic mixtures and the role of electrolyte, J. Coll. Int. Sci. 516 (2018) 456–465.
[13] H. Xu, P.X. Li, K. Ma, R.J.L. Welbourn, J. Penfold, R.K. Thomas, D.W. Roberts, J.T. Petkov, The role of competitive counterion adsorption on the electrolyte induced surface ordering in methyl ester sulfonate surfactants at the air-water interface, J. Coll. Int. Sci. 533 (2019) 154–160.
[14] Z. Wang, P.X. Li, K. Ma, Y. Chen, M. Campana, J. Penfold, R.K. Thomas, D.W. Roberts, H. Xu, J.T. Petkov, Z. Yan, Impact of molecular structure, headgroup and alkyl chain geometry on the adsorption of the anionic sulfonate surfactants at the air-solution interface, in the presence and absence of electrolyte, J. Coll. Int. Sci. 544 (2019) 293–302.
[15] Z. Wang, P.X. Li, K. Ma, Y. Chen, Z. Yan, J. Penfold, R.K. Thomas, M. Campana, J.R.P. Webster, Z. Li, J.H. Neil, J.T. Petkov, D.W. Roberts, α-sulfo alkyl ester surfactants: impact of changing the alkyl chain length on the adsorption, mixing properties and response to electrolyte of the tetradecanoate, J. Coll. Int. Sci. 585 (2021) 876–890.
[16] L.R. Griffin, K.L. Browning, S.Y. Lee, M.W.A. Skoda, S. Rogers, S.M. Clarke, Multilayering of Ca AOT at the mica/water interface studies with neutron reflectivity: formation of a condensed lamellar phase at the cmc, Langmuir 32 (2016) 13054–13064.
[17] L.J. Allan, C.L. Truscott, P. Gutfreund, R.J.L. Welbourn, S.M. Clarke, Potassium, calcium and magnesium bridging of AOT to mica at constant ionic strength, Langmuir 35 (2019) 5753–5761.

[18] J. Penfold, D.S. Sivia, E. Staples, I. Tucker, R.K. Thomas, Surface ordering in dilute dihexadecyl dimethyl ammonium bromide solutions at the air-water interface, Langmuir 20 (2004) 2265–2269.
[19] Z.X. Li, J.R. Lu, R.K. Thomas, J. Penfold, Neutron specular and off-specular reflection from the surface of aerosol-OT solutions above the cmc, Faraday Discussion 104 (1996) 127–138.
[20] Z.X. Li, A. Weller, R.K. Thomas, A.R. Rennie, J.R.P. Webster, J. Penfold, R.K. Heenan, R. Cubitt, Adsorption of the lamellar phase of aerosol-OT at the solid-liquid and air-liquid interfaces, J. Phys. Chem. B 103 (1999) 10800–10806.
[21] Z.X. Li, J.R. Lu, R.K. Thomas, A. Weller, J. Penfold, J.R.P. Webster, D.S. Sivia, A.R. Rennie, Conformal roughness in the adsorbed lamellar phase of aerosol-OT at the air-water and liquid-solid interfaces, Langmuir 17 (2001) 5858–5864.
[22] D.J. McGillivray, R.K. Thomas, A.R. Rennie, J. Penfold, D.S. Sivia, Ordered structures of di-chain cationic surfactants at interfaces, Langmuir 19 (2003) 7719–7726.
[23] R.J.L. Welbourn, F. Bartholomew, P. Gutfreund, S.M. Clarke, Neutron reflectivity of an anionic surfactant at the solid-liquid interface under shear, Langmuir 33 (2017) 5982–5990.
[24] M.S. Hellsing, A.R. Rennie, A.V. Hughes, Adsorption of Aerosol-OT to sapphire: lamellar structure studied with neutrons, Langmuir 27 (2011) 4669–4678.
[25] J. Penfold, R.K. Thomas, C.C. Dong, I. Tucker, K. Metcalfe, S. Golding, I. Grillo, Equilibrium surface adsorption behaviour in complex anionic/nonionic surfactant mixtures, Langmuir 23 (2007) 10140–10149.
[26] I. Tucker, J. Penfold, R.K. Thomas, C.C. Dong, S. Golding, C. Gibson, I. Grillo, Surface and solution properties of anionic/nonionic surfactant mixtures of alkyl benzene sulfonate and triethylene glycol dodecyl ether, Langmuir 26 (2010) 10614–10626.
[27] I. Tucker, J. Penfold, R.K. Thomas, C.C. Dong, S. Golding, C. Gibson, I. Grillo, The adsorption and self-assembly of mixtures of alkyl benzene sulfonate isomers and the role of divalent electrolyte, Langmuir 27 (2011) 6674–6682.
[28] S.P. Moulik, K. Mukkerjee, On the versatile surfactant aerosol-OT, its physicochemical and surface chemical behaviour and uses, Proc. Indian Natn. Sci. Acad. 62 (1996) 215–232.
[29] F. Candau, V.S. Leung, G. Pouyet, S. Candau, Inverse microemulsion polymerisation of acrylamide: characterisation of a water-in-oil microemulsion and the final microlatexes, J. Coll. Int. Sci. 101 (1984) 167–183.
[30] J. Eastoe, G. Fragneto, B.H. Robinson, T.F. Toney, R.K. Heenan, L.J. Leng, Variation of surfactant counterions and its effect on the structure and properties of Aerosol-OT based water-in-oil microemulsions, J. Chem. Soc. Faraday Trans. 88 (1992) 461–471.
[31] J.K. Hensel, A.P. Carpenter, R.K. Ciszewski, B.K. Schaber, C.T. Kitteridge, F.G. Moore, G.L. Richmond, Molecular characterisation of water and surfactant AOT at nanoemulsion surfaces, Proc. Nat. Acad. Sci. 114 (2017) 13351–13356.
[32] K. Fontell, The structure of the lamellar liquid crystalline phase of Aerosol-OT-water system, J. Coll. Int. Sci. 44 (1973) 318–329.
[33] J. Rogers, P.A. Winsor, Change in optic sign of the lamellar phase in the Aerosol-OT/water system with composition or temperature, J. Coll. Int. Sci. 30 (1969) 247–257.
[34] D. Park, J. Rogers, R.W. Topt, P.A. Winsor, The structure of micellar solutions of ionic amphiphile. The lamellar phase. X-ray diffraction measurements with the Aerosol-OF/water system, J. Coll. Int. Sci. 32 (1970) 81–89.
[35] M. Skouri, J. Marignan, R. May, X-ray and neutron scattering study of the lamellar and L_3 phases of the system aerosol-OT/water: effect of NaCl and decane, Coll. Polym. Sci. 269 (1991) 929–937.
[36] P. Petrov, U. Olsson, H. Christenson, S. Miklavic, H. Wennerstrom, Forces between macroscopic surfaces in a sponge phase, Langmuir 10 (1994) 988–990.
[37] O. Ghosh, C.A. Miller, Liquid crystalline and microemulsion phase behaviour in alcohol free Aerosol-OT/oil/brine systems, J. Phys. Chem. 91 (1987) 4528–4535.
[38] A. Khan, B. Jensson, H. Wennerstrom, Phase equilibria in mixed sodium and calcium di-2-ethylhexyl sulfosuccinate aqueous systems: and illustration of repulsive and attractive double layer forces, J. Phys. Chem. 89 (1985) 5180–5184.
[39] Z.X. Li, J.R. Lu, R.K. Thomas, Neutron reflectivity studies of the adsorption of AOT at the air/water interface: the surface excess, Langmuir 13 (1997) 3681–3685.
[40] J. Eastoe, S. Nave, A. Downer, A. Paul, A. Rankin, K. Tribe, J. Penfold, Adsorption of ionic surfactants at the air-solution interface, Langmuir 16 (2000) 4511–4518.
[41] CRISP reflectometer at the ISIS neutron source, https://www.isis.stfc.ac.uk/pages/crisp.aspx
[42] SURF reflectometer at the ISIS neutron source, https://www.isis.stfc.ac.uk/pages/surf.aspx
[43] ISIS Deuteration Facility, https://www.isis.stfc.ac.uk/pages/ISIS-Deuteration-Facility.aspx
[44] Z.X. Li, R.K. Thomas, J. Penfold, NR studies on the adsorption of AOT at the air-water interface: the structure of the sodium salt, J. Phys. Chem. B 101 (1997) 1615–1620.
[45] H. Xu, P.X. Li, K. Ma, R.K. Thomas, J. Penfold, J.R. Lu, Limitations in the application of the Gibbs equation to anionic surfactants at the air-water interface: sodium dodecylsulfate and sodium dodecylmonooxyethylene sulfate above and below the cmc, Langmuir 29 (2013) 9335–9351.
[46] R.K. Thomas, J. Penfold, Thermodynamics of the air-water interface of mixtures of surfactants with polyelectrolytes, oligoelectrolytes and multivalent metal electrolytes, J. Phys. Chem. B 122 (2018) 12411–12427.
[47] J.R. Lu, R.K. Thomas, J. Penfold, Surfactant layers at the air-waer interface: structure and composition, Adv. Coll. Int. Sci. 2000, 84, 143-304
[48] H. Xu, P.X. Li, K. Ma, R.J.L. Welbourn, J. Penfold, D.W. Roberts, R.K. Thomas, J.T. Petkov, Adsorption of methyl ester sulfonate at the air-water interface: can limitations in the application of the Gibbs equation be overcome by computer purification, Langmuir 33 (2017) 9944–9953.
[49] J. Penfold, R.K. Thomas, The application of the specular reflection of neutrons to the study of surfaces and interfaces, J. Phys.: Condens. Matt. 2 (1990) 1369–1412.
[50] I.M. Tidswell, B.M. Ocko, P.S. Pershan, S.R. Wassermann, G.M. Whitesides, J.D. Axe, X-ray reflection studies of silicon coated by organic monolayers (alkyl siloxanes), Phys. Rev. B 41 (1990) 1111–1128.
[51] S.K. Sinha, M.K. Sanyal, S.K. Satija, C.F. Majkrzak, D.A. Neumann, H. Homma, S. Szpala, H. Gibaud, H. Morkov, X-ray scattering studies f surface roughness of GaAs/AlAs multilayers, Phys. B 198 (1994) 72–77.
[52] D.S. Sivia, J.R.P. Webster, The Bayesian approach to reflectivity data, Phys. B 248 (1991) 327–337.
[53] A. Maneedaeng, K.J. Haller, B.P. Grady, A.E. Flood, Thermodynamic parameters and counterion binding to the micelle in binary anionic surfactants, J. Coll. Int. Sci. 356 (2011) 598–604.
[54] K.L. Steller, J.F. Scamehorn, Surfactant precipitation in aqueous solutions containg mixtures of anionic and nonionic surfactants, J. Am. Oil Chem. Soc. 63 (1986) 366–370.
[55] P. Paton-Morales, F.I. Talens-Allesson, Effect of ionic strength and competitive adsorption of Na^+ on the flocculation of Lauryl sulfate micelles with Al^{3+}, Langmuir 17 (2001) 6059–6064.
[56] R.G. Alargova, J.T. Petkov, D.N. Petsev, Micellisation and interfacial properties of alkyloxyethylene sulfate surfactant solutions in the presence of multivalent counterions, J. Coll. Int. Sci. 261 (2003) 1–11.
[57] D. Kashchiev, D.E. Exerowa, Structure and surface energy of surfactant layers in the alveolar surface, Eur. J. Biophys. 30 (2001) 34–41.